Solar Cells

Deutsche Ausgabe: DOI: 10.1002/ange.201602545
Internationale Ausgabe: DOI: 10.1002/anie.201602545

Highly Efficient Perovskite Solar Cells Employing an Easily Attainable Bifluorenylidene-Based Hole-Transporting Material

*Kasparas Rakstys, Michael Saliba, Peng Gao, Paul Gratia, Egidijus Kamarauskas, Sanghyun Paek, Vygintas Jankauskas, and Mohammad Khaja Nazeeruddin**

Abstract: *The 4,4′-dimethoxydiphenylamine-substituted 9,9′-bifluorenylidene (**KR216**) hole transporting material has been synthesized using a straightforward two-step procedure from commercially available and inexpensive starting reagents, mimicking the synthetically challenging 9,9′-spirobifluorene moiety of the well-studied spiro-OMeTAD. A power conversion efficiency of 17.8 % has been reached employing a novel HTM in a perovskite solar cells.*

Perovskite-based solar cells (PSCs) have rapidly become the hottest topic in photovoltaics due to their unique optical and electrical properties, since the first report in 2009 by Miyasaka et al.[1] The best performing device configuration of PSC is composed of an electron-transporting material (ETM), typically a mesoporous layer of TiO_2, which is infiltrated with perovskite absorber material, coated with a hole-transporting material (HTM) and gold as a back contact.[2–5]

Numerous organic small molecule-based HTMs have been explored in PSCs, reaching efficiency of 16–18 %.[6–11] To date, 2,2′,7,7′-tetrakis(*N*,*N*-di-*p*-methoxyphenylamine)-9,9′-spirobifluorene (spiro-OMeTAD) and 2′,7′-bis(bis(4-methoxyphenyl) amino) spiro[cyclopenta[2,1-*b*:3,4-*b*′]dithiophene-4,9′-fluorene] (FDT) HTMs reached the highest reported values over 20 %.[12,13] However, the multi-step synthesis of spiro-type derivatives is prohibitively expensive and challenging, since it requires low temperature and harsh acidic and basic conditions. Moreover, high-purity sublimation-grade spiro-OMeTAD is required to obtain high-performance devices.

Here we present a molecularly engineered HTM 4,4′-dimethoxydiphenylamine-substituted 9,9′-bifluorenylidene **KR216** with performance on par with that of spiro-OMeTAD. In addition, the novel HTM does not require an expensive synthetic procedure and was prepared employing a straightforward two-step strategy. 9-Fluorenylidene moiety is known to facilitate charge carrier migration conveying electrons from donor to acceptor throughout the structure and have never been tested as potential HTMs for PSC.[14]

The general synthesis procedure for the preparation of 2,2′,7,7′-tetrakis(*N*,*N*-di-*p*-methoxyphenylamine)-9,9′-bifluorenylidene **KR216** is shown in Scheme 1. Commercially available and inexpensive precursor 2,7-dibromo-9*H*-fluoren-9-one have been reacted with 2,4-bis(4-methoxyphenyl)-1,3,2,4-dithiadiphosphetane-2,4-dithione, well known as Lawesson's reagent, to form 9,9′-ylidene (C=C) double bond. With this we demonstrate the synthesis of 2,2′,7,7′-tetrabromo-9,9′-bifluorenylidene **1** by single-step reaction, accelerating the synthetic routes proposed by Wudl and Luh, using dimerization of the substituted 9-bromofluorene in the presence of DBU and desulfurdimerization of dithioketals mediated by $W(CO)_6$, respectively.[15,16] Furthermore, we note that no column chromatography was required in advance for the next step. Then, the symmetrical olefin have been equipped with 4,4′-dimethoxydiphenylamine units using the palladium-catalyzed Buchwald–Hartwig C–N cross-coupling reaction, to release final HTM **KR216** having 9,9′-bifluorenylidene central core, which mimics 9,9′-spirobifluorene moiety of well-studied spiro-OMeTAD.

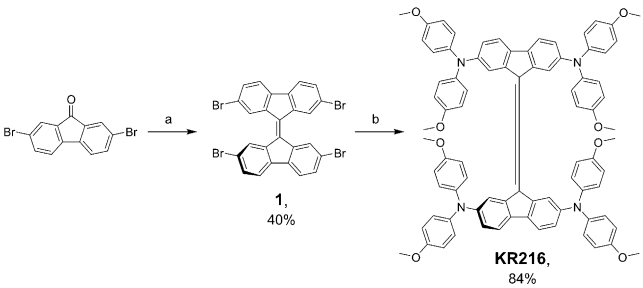

Scheme 1. Straightforward synthetic route for the **KR216** HTM. a) Lawesson's reagent, toluene, 110 °C. b) 4,4′-Dimethoxydiphenylamine, *t*-BuONa, Pd_2dba_3, XPhos, toluene, 110 °C.

It is well known, that both organic impurities and metal residues may present in final raw organic semiconducting materials, and they are known to act as charge carrier traps or photoquenchers significantly affecting their original properties, consequently reducing the photovoltaic performance.[17,18] Therefore, we have synthesized spiro-OMeTAD in our lab under the same final cross-coupling step and

[*] K. Rakstys, Dr. M. Saliba, Dr. P. Gao, P. Gratia, Dr. S. Paek, Prof. Dr. M. K. Nazeeruddin
Group for Molecular Engineering of Functional Materials
Institute of Chemical Sciences and Engineering
École Polytechnique Fédérale de Lausanne
1015 Lausanne (Switzerland)
E-mail: mdkhaja.nazzeruddin@epfl.ch
E. Kamarauskas, Dr. V. Jankauskas
Department of Solid State Electronics
Vilnius University
Sauletekio 9, Vilnius, 10222 (Lithuania)
Prof. Dr. M. K. Nazeeruddin
Center of Excellence for Advanced Materials Research
King Abdulaziz University
Jeddah (Saudi Arabia)

Supporting information for this article can be found under: http://dx.doi.org/10.1002/anie.201602545.

purified using both flash chromatography and precipitation procedures as for **KR216**, having the same purity grade in order to achieve a more accurate comparison. All synthetic procedures and cost estimation are reported in the Supporting Information.

The chemical structure of **KR216** is confirmed by X-ray diffraction analysis as displayed in Figure 1 a. Similar to the ubiquitous spiro-OMeTAD, four diphenyl amine units are attached to the two central fluorene skeletons with four different torsion angles with the minimum of 15.2° and the maximum of 83°. This is an indication of different degree of distortion among the four bulky propeller shaped diphenyl amine units. This can be understood by Figure 1 b, in which the crystal structure of **KR216** is found to be distinct from that of spiro-OMeTAD, when the sp^3 carbon atom in the latter is replaced by a double bond between two sp^2 hybridized carbon atoms.[19] It is known that the sp^2 hybridized π bond cannot rotate freely and tend to form either *cis*- or *trans*-conformation. So the competition between the planarization and repulsive steric hindrance lead to a pseudo *spiro* conformation and diversified torsion angles. Therefore, the dihedral angles between the two double-bond connected fluorenes are measured to be either 42.4° (43.7°) or 35.4° (36.5°). These values are much smaller than that of spiro-OMeTAD (89.94°) due to the reason mentioned above (Figure S7-a). This effect is also reflected in the length of double bond between two fluorenes, the value of which is also varied according to the degree of distortion (Figure S7-b).

KR216 was found to crystallize in the triclinic space group *P*1. In one unit cell, four independent molecules the crystal lattice stacked in a highly slipped fashion (Figure 1 c,d) through π···π, C···C and C···O short contacts as well as CH/π (CH/O) hydrogen bonds. Eight fluorenes are found to have three different types of orientation. As indicated in Figure 1 c the parallel fluorenes with same orientation is marked with the same color. When scrutinizing the crystal structure of **KR216**, an abundance of non-covalent intermolecular interactions are found with shortest π···π distance of 3.378 Å, shortest C···C contacts of 3.254 Å and shortest C···O contacts of 3.090 Å. Similar to that of spiro-OMeTAD, due to the highly sterically hindered geometry, no close face to face overlap is observed. However, the small π···π distance[20] and short C···O contacts are expected to facilitate the facile establishment of highly efficient charge transport channel.

The thermal behavior of HTMs was determined by thermogravimetric analysis (TGA) and differential scanning calorimetry (DSC) measurements (Table 1). From TGA, it was found that **KR216** has a similar to spiro-OMeTAD (417 °C) and relatively high decomposition temperature (T_{dec}) of 398 °C, with a weight loss of 5 %, indicating good thermal stability, required for photovoltaic devices.

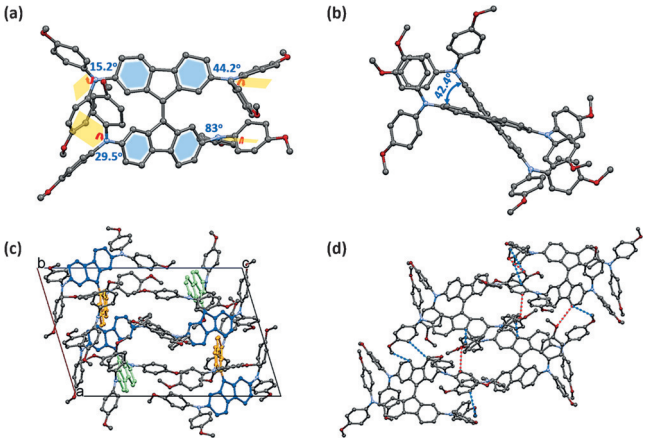

Figure 1. a) ORTEP drawings of **KR216** determined by X-ray crystallography indicating four different kinds of dihedral angles between the two central fluorenes and four diphenyl amine units (hydrogen atoms omitted for clarity). b) Perspective views of **KR216** molecule showing one typical dihedral angle between the two fluorene units (42.4°). c) View down reciprocal cell axis b of the stacking molecules showing three different types of orientation of the eight fluorene units (same orientation with same color). d) Noncovalent intermolecular short contacts of **KR216** in a one-unit cell. Dashed blue lines illustrate π···π short contacts (3.378 Å, and 3.381 Å) and C···C short contacts (3.254 Å, 3.313 Å, 3.336 Å, 3.340 Å, 3.350 Å, and 3.370 Å,). Dashed red lines illustrate C···O short contacts (3.090 Å, 3.105 Å, 3.185 Å and 3.180 Å).

Table 1: Thermal properties of **KR216** and spiro-OMeTAD.

ID	T_m [°C][a]	T_g [°C][a]	T_{cr} [°C][a]	T_{dec} [°C][b]
KR216	309	157	228	398
spiro-OMeTAD	234	126	–	417

[a] Melting, glass transition, and crystallization temperatures observed from DSC (10 °C min^{-1}, Ar atmosphere). [b] Degradation temperature observed from TGA (5 % weight loss at 10 °C min^{-1}, N_2 atmosphere).

The thermal transitions of **KR216** were studied by DSC and compared with spiro-OMeTAD (Figure 2). During the first heating scan, both glass transition (T_g) (157 °C) and melting of the crystals (309 °C) are observed, indicating that the material could exist in both crystalline and amorphous states. Additionally, crystallization process is detected at 228 °C, whereas no crystallization was observed during the cooling and second heating steps, only the glass transition at 157 °C.

Similarly to **KR216**, spiro-OMeTAD can also exist in both amorphous and crystalline states.[21] During the first heating, no crystallization and only melting was detected at 234 °C. The glass transition of spiro-OMeTAD was observed only during the second heating cycle at 126 °C and is lower than that of **KR216**, indicating that **KR216** has more stabilized amorphous state.

The normalized UV/Vis absorption spectra of **KR216** and spiro-OMeTAD in THF are shown in Figure 3. Both exhibit almost identical absorption band in UV region with the absorption maximum at 390 nm, while the **KR216** also shows a broad optical absorption in the visible region centered at 466 nm, revealing enhanced conjugation through 9-ylidene double bond with better π-electron delocalization. Optical band gaps (E_g) determined from the onset of absorption were 2.41 eV for **KR216** and 3.00 eV for spiro-OMeTAD, respectively.

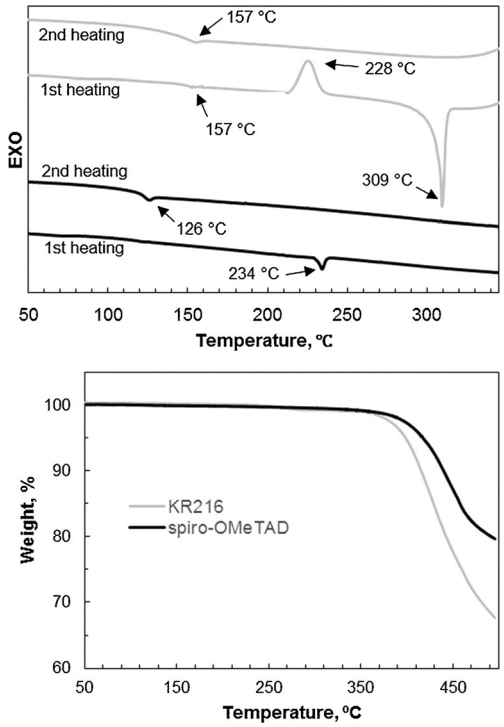

Figure 2. DSC first and second heating curves of **KR216** and spiro-OMeTAD, scan rate 10 °C min^{-1}, Ar atmosphere (top). Thermogravimetric analysis (TGA) data of HTMs, heating rate of 10 °C min^{-1}, N_2 atmosphere (down).

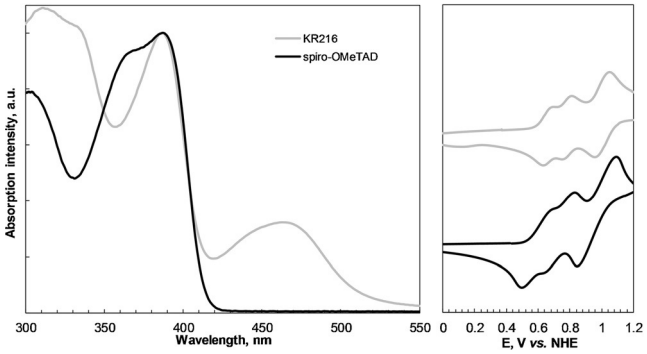

Figure 3. UV/Vis absorption spectra normalized at the peak value (left) and cyclic voltammograms (right) of **KR216** and spiro-OMeTAD.

To compare the energy levels of the new HTM with spiro-OMeTAD we performed cyclic voltammetry (CV) measurements. The data derived from the ground-state oxidation potential (E^{HOMO}) estimated from the cyclic voltammogram shown in Figure 3 are summarized in Table 2. No reduction potential was observed in the CV measurement. The HOMO value of **KR216** was estimated to be −5.09 eV versus the vacuum, which is slightly destabilized compared with that of spiro-OMeTAD (−5.04 eV). However, the 5 meV difference is small and hardly affects the hole transfer from the perovskite (−5.65 eV)[22] to the **KR216**.

To elucidate the influence of impurities for energy and electron transfer, electrical properties were determined using both grades of spiro-OMeTAD and comparing with the

Table 2: Optical and electrochemical properties comparison.

ID	λ_{abs} [nm][a]	E_g [eV][b]	E^{HOMO} vs. NHE [V][c]	HOMO vs. vacuum [eV][c]	LUMO [eV][d]
KR216	390, 466	2.41	0.65	−5.09	−2.68
spiro-OMeTAD	390	3.00	0.60	−5.04	−2.04

[a] Absorption was measured in THF solution. [b] Determined from the UV/Vis absorption onset. [c] Measured in DCM/tetra-*n*-butylammonium hexafluorophosphate (0.1 M) solution, using glassy carbon working electrode, Pt reference electrode, and Pt counter electrode with Fc/Fc^+ as an internal standard. Potentials were converted to the normal hydrogen electrode by addition of +0.624 V and −4.44 eV to the vacuum, respectively. [d] Calculated from LUMO = HOMO + E_g.

KR216. The solid-state ionization potential (I_P) was measured by the electron photoemission in air on the thin films (PESA, Figure S9). **KR216** and spiro-OMeTAD have similar I_P values, 5.01 and 5.10, respectively. The small 0.07 eV difference was noticed to ionize different grade spiro-OMeTAD samples. Lateral thin-film conductivity of HTM layers was measured on OFET substrates (Figure S10). The conductivity of oxidized **KR216** was determined to be 3.40×10^{-5} S cm^{-1}, which is slightly higher of that of lab-grade spiro-OMeTAD ($\sigma = 3.04\times10^{-5}$ S cm^{-1}). More than two times higher conductivity was obtained for commercial spiro-OMeTAD ($\sigma = 6.89\times10^{-5}$ S cm^{-1}), showing a huge negative influence of remained impurities. Xerographic time-of-flight (XTOF) measurements were used to characterize charge-transporting properties of the HTMs (Figures S11, S12). Gaussian-type hole transport with well-defined transit time was observed in **KR216**. The room-temperature zero-field hole-drift mobility of **KR216** was measured to be 4.6×10^{-5} cm^2 V^{-1} s^{-1} and indicates similar charge hopping properties as for spiro-OMeTAD ($\mu_0 = 1\times10^{-4}$ cm^2 V^{-1} s^{-1}). Similarly to conductivity results, high-purity commercial spiro-OMeTAD has higher hole-drift mobility, reaching 1.3×10^{-4} cm^2 V^{-1} s^{-1}. All electrical properties are summarized in Table 3.

Table 3: Comparison of electrical properties.

ID	I_P [eV][a]	μ_0 [cm^2 V^{-1} s^{-1}][b]	μ [cm^2 V^{-1} s^{-1}][c]	σ [S cm^{-1}][d]
KR216	5.01	4.6×10^{-15}	7.0×10^{-4}	3.40×10^{-5}
spiro-OMeTAD synthesized	5.10	1×10^{-4}	1×10^{-3}	3.04×10^{-5}
spiro-OMeTAD commercial	5.03	1.3×10^{-4}	2.1×10^{-3}	6.89×10^{-5}

[a] Ionization potential was measured by the photoemission in air method from films. [b] Hole mobility value at zero field strength. [c] Hole mobility value at 3.6×10^5 V cm^{-1} field strength. [d] Conductivity was measured using 70 mM HTMs solution in chlorobenzene, doped with 3 mol% FK209.

To demonstrate the ability of **KR216** act as HTM, we prepared PSCs with perovskite as the absorber and compared with the cells fabricated using the both grades of spiro-OMeTAD under similar conditions. The HTM layers were deposited onto the mixed perovskite from a chlorobenzene solution containing 330 mol% *tert*-butylpyridine (TBP),

50 mol% tris(bis(trifluoromethylsulfonyl)imide) (Li-TFSI) and 3 mol% FK209 (Co^{III} oxidant) as additives. Detailed device fabrication procedure is outlined in SI. The current density–voltage (*J–V*) curves of the best devices under 100 mW cm^{-2} AM1.5G solar illumination with reverse and forward scans are shown in Figure 4, and the extracted corresponding parameters are summarized in Table 4. Our

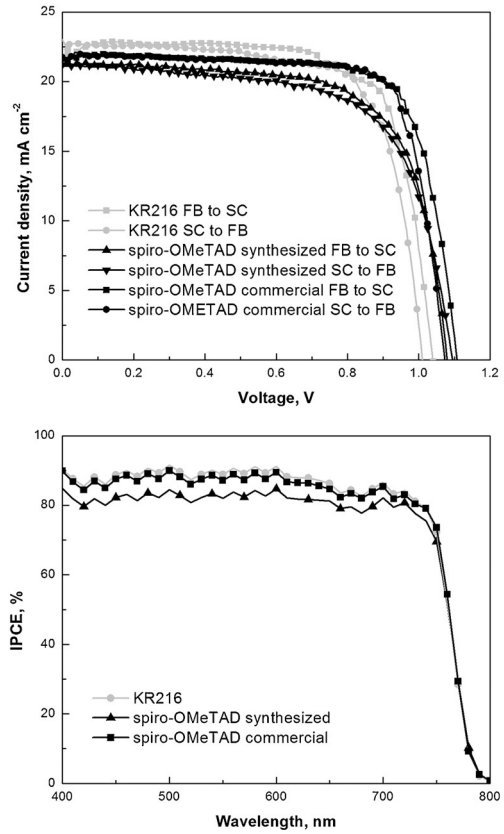

Figure 4. *J–V* curves of best performing devices prepared with **KR216** and spiro-OMeTAD as the reference. Devices were masked with a black metal aperture of 0.16 cm^2 to define the active area. The curves were recorded scanning at 0.01 V s^{-1} (top) and IPCE spectra as a function of the wavelength of monochromatic light (down).

Table 4: Solar-cell performance parameters, extracted from *J–V* curves.

ID	Scan direction	J_{SC} [mA cm^{-2}]	V_{OC} [mV]	FF	PCE [%]
KR216	FB to SC	22.3	1023	0.77	17.8
	SC to FB	22.4	1004	0.74	16.8
spiro-OMeTAD	FB to SC	20.6	1090	0.75	17.4
synthesized	SC to FB	20.7	1080	0.72	16.3
spiro-OMeTAD	FB to SC	21.4	1107	0.76	18.4
commercial	SC to FB	21.7	1073	0.77	18.4

measurements were taken at a slow scan rate of 10 mV s^{-1}, resembling quasi steady-state conditions.[23,24] The device with **KR216** as HTM possesses an open-circuit voltage (V_{OC}) of 1023 mV, a short circuit current density (Jsc) of 22.3 mA cm^{-2}, and a fill factor (FF) of 0.77, yielding PCE of 17.8% for the forward and 1004 mV, 22.4 mA cm^{-2}, 0.74, 16.8% in backward scan, respectively. In comparison, it is slightly higher than that of device prepared with our lab-grade spiro-OMeTAD, 17.4% for forward and 16.3% in backward scan, respectively. This result clearly shows that **KR216** is an excellent HTM for PSC.

Improved photovoltaic performance reaching PCE of 18.4% was observed of the device built on high-purity commercial spiro-OMeTAD under identical conditions. Despite, higher V_{OC}, J_{SC}, and FF yielding higher overall efficiency, there are also less difference obtained between the forward and reverse scans, confirming that high-purity of spiro-OMeTAD is required to obtain high-performance devices. Furthermore, we note that the optimized perovskite contributed towards the high efficiencies in this work.

The incident photon-to-current efficiency (IPCE) (Figure 4) of the perovskite devices as a function of wavelength shows that the device with **KR216** as the HTM exhibits IPCE above 85% from 400 nm covering all the visible region to 700 nm. Photocurrents obtained from the IPCE data are in close agreement with those of current–voltage measurements.

In conclusion, we report a novel easily attainable 9,9′-bifluorenylidene-based hole-transporting material named **KR216**, obtained by a straightforward two-step synthetic route from commercially available and inexpensive starting materials. The estimated price of **KR216** is around 50 times lower than that of commercial spiro-OMeTAD. A remarkable power conversion efficiency of 17.8% was obtained for perovskite solar cells using **KR216**, which is on par with the power conversion efficiency of the high-purity commercial spiro-OMeTAD. The presented result clearly demonstrates that the 9-fluorenylidene moiety is very promising for future molecular engineering of HTMs and let us believe that **KR216** has a potential for commercial application in high-performance PSC.

Acknowledgements

The research leading to these results received funding from the Qatar National Research Fund (grant number NPRP 6-1752-070; a member of The Qatar Foundation). M.S. acknowledges support from the co-funded Marie Skłodowska Curie fellowship, H2020 grant agreement number 665667. We thank the Swiss State Secretariat for Education, Research and Innovation (SERI), CEPF Special Energy Fund for EPFL-Sion, and Prof. Michael Grätzel for allowing to use LPI facilities.

Keywords: bifluorenylidene · electrochemistry · hole-transporting materials · photovoltaics · solar cells

How to cite: *Angew. Chem. Int. Ed.* **2016**, *55*, 7464–7468
Angew. Chem. **2016**, *128*, 7590–7594

[1] A. Kojima, K. Teshima, Y. Shirai, T. Miyasaka, *J. Am. Chem. Soc.* **2009**, *131*, 6050.
[2] H. S. Kim, C. R. Lee, J. H. Im, K. B. Lee, T. Moehl, A. Marchioro, S. J. Moon, R. Humphry-Baker, J. H. Yum, J. E. Moser, M. Grätzel, N. G. Park, *Sci. Rep.* **2012**, *2*, 591.

[3] J. H. Heo, S. H. Im, J. H. Noh, T. N. Mandal, C.-S. Lim, J. A. Chang, Y. H. Lee, H. Kim, A. Sarkar, M. K. Nazeeruddin, M. Grätzel, S. Il Seok, *Nat. Photonics* **2013**, *7*, 486.
[4] J. H. Noh, S. H. Im, J. H. Heo, T. N. Mandal, S. Il Seok, *Nano Lett.* **2013**, *13*, 1764.
[5] P. Gao, M. Grätzel, M. K. Nazeeruddin, *Energy Environ. Sci.* **2014**, *7*, 2448.
[6] P. Gratia, A. Magomedov, T. Malinauskas, M. Daskeviciene, A. Abate, S. Ahmad, M. Grätzel, V. Getautis, M. K. Nazeeruddin, *Angew. Chem. Int. Ed.* **2015**, *54*, 11409; *Angew. Chem.* **2015**, *127*, 11571.
[7] M. H. Li, C. W. Hsu, P. S. Shen, H. M. Cheng, Y. Chi, P. Chen, T. F. Guo, *Chem. Commun.* **2015**, *51*, 15518.
[8] S. Park, J. H. Heo, C. H. Cheon, H. Kim, S. H. Im, H. J. Son, *J. Mater. Chem. A* **2015**, *3*, 24215.
[9] Y. Liu, Z. Hong, Q. Chen, H. Chen, W. H. Chang, Y. Yang, T. B. Song, Y. Yang, *Adv. Mater.* **2016**, *28*, 440.
[10] H. Nishimura, N. Ishida, A. Shimazaki, A. Wakamiya, A. Saeki, L. T. Scott, Y. Murata, *J. Am. Chem. Soc.* **2015**, *137*, 15656.
[11] K. Rakstys, A. Abate, M. I. Dar, P. Gao, V. Jankauskas, G. Jacopin, E. Kamarauskas, S. Kazim, S. Ahmad, M. Grätzel, M. K. Nazeeruddin, *J. Am. Chem. Soc.* **2015**, *137*, 16172.
[12] D. Bi, W. Tress, M. I. Dar, P. Gao, J. Luo, C. Renevier, K. Schenk, A. Abate, F. Giordano, J. P. C. Baena, J. D. Decoppet, S. M. Zakeeruddin, M. K. Nazeeruddin, M. Grätzel, A. Hagfeldt, *Sci. Adv.* **2016**, *2*, e1501170.
[13] M. Saliba, S. Orlandi, T. Matsui, S. Aghazada, M. Cavazzini, J. P. Correa-Baena, P. Gao, R. Scopelliti, E. Mosconi, K. H. Dahmen, F. De Angelis, A. Abate, A. Hagfeldt, G. Pozzi, M. Graetzel, M. K. Nazeeruddin, *Nat. Energy* **2016**, *1*, 15017.
[14] G. L. Eakins, M. W. Cooper, N. N. Gerasimchuk, T. J. Phillips, B. E. Breyfogle, C. J. Stearman, *Can. J. Chem.* **2013**, *91*, 1059.
[15] F. G. Brunetti, X. Gong, M. Tong, A. J. Heeger, F. Wudl, *Angew. Chem. Int. Ed.* **2010**, *49*, 532; *Angew. Chem.* **2010**, *122*, 542.
[16] L. L. Yeung, Y. C. Yip, T. Y. Luh, *J. Org. Chem.* **1990**, *55*, 1874.
[17] M. Degbia, M. Ben Manaa, B. Schmaltz, N. Berton, J. Bouclé, R. Antony, F. Tran Van, *Mater. Sci. Semicond. Process.* **2016**, *43*, 90.
[18] Ö. Usluer, M. Abbas, G. Wantz, L. Vignau, L. Hirsch, E. Grana, C. Brochon, E. Cloutet, G. Hadziioannou, *ACS Macro Lett.* **2014**, *3*, 1134.
[19] P. Ganesan, K. Fu, P. Gao, I. Raabe, K. Schenk, R. Scopelliti, J. Luo, L. H. Wong, M. Grätzel, M. K. Nazeeruddin, *Energy Environ. Sci.* **2015**, *8*, 1986.
[20] K. Avasthi, L. Shukla, R. Kant, K. Ravikumar, *Acta Crystallogr. Sect. C* **2014**, *70*, 555.
[21] T. Malinauskas, D. Tomkutė-Lukšienė, R. Sens, M. Daskeviciene, R. Send, H. Wonneberger, V. Jankauskas, I. Bruder, V. Getautis, *ACS Appl. Mater. Interfaces* **2015**, *7*, 11107.
[22] J. P. C. Baena, L. Steier, W. Tress, M. Saliba, S. Neutzner, T. Matsui, F. Giordano, T. J. Jacobsson, A. R. S. Kandada, S. M. Zakeeruddin, A. Petrozza, A. Abate, M. K. Nazeeruddin, M. Graetzel, A. Hagfeldt, *Energy Environ. Sci.* **2015**, *8*, 2928.
[23] E. L. Unger, E. T. Hoke, C. D. Bailie, W. H. Nguyen, A. R. Bowring, T. Heumüller, M. G. Christoforod, M. D. McGehee, *Energy Environ. Sci.* **2014**, *7*, 3690.
[24] J. A. Christians, J. S. Manser, P. V. Kamat, *J. Phys. Chem. Lett.* **2015**, *6*, 852.

Received: March 12, 2016
Revised: April 1, 2016
Published online: May 9, 2016

